JOC The Journal of Organic Chemistry

Article

pubs.acs.org/joc

Synthesis, Structure, Electrochemistry, and Electrochemiluminescence of Thienyltriazoles

Kalen N. Swanick, Jacquelyn T. Price, Nathan D. Jones, and Zhifeng Ding*

Department of Chemistry, The University of Western Ontario, 1151 Richmond Street, London, Ontario, Canada N6A 5B7

Supporting Information

ABSTRACT: Four blue-emitting thienyltriazoles with desired N and O coordination atoms were prepared in high yield via click chemistry for potential incorporation into metal complexes. Three of their crystal structures were determined by X-ray crystallography. The electrochemical properties, electronic structures of these thienyltriazoles, **1**−**4**, and their correlations were studied using cyclic voltammetry and differential pulse voltammetry techniques along with density function theory (DFT) calculations. All of the compounds underwent irreversible redox reactions, leading to unstable electrogenerated radical cations and anions. Electrochemical gaps determined from the differences between first formal reduction and oxidation reactions were correlated to HOMO−LUMO energy gaps obtained from UV−vis spectroscopy and the DFT calculations as well as energies of excited states measured from photoluminescence spectroscopy. We observed weak electrochemiluminescence (ECL) from annihilation of these thienyltriazole radicals in acetonitrile containing 0.1 M tetra-*n*-butylammonium perchlorate as electrolyte. An enhancement in ECL efficiency ranging from 0.16 to 0.50% was observed upon addition of benzoyl peroxide as a coreactant in the above electrolyte solutions. The generation of excimers in solutions of **1**−**4** was observed as seen by the red-shift in ECL maxima relative to their corresponding photoluminescence peak wavelengths. Our work is of importance for the development of efficient blue-emitting fluorophores via click chemistry that could be potential luminophores in metal complexes.

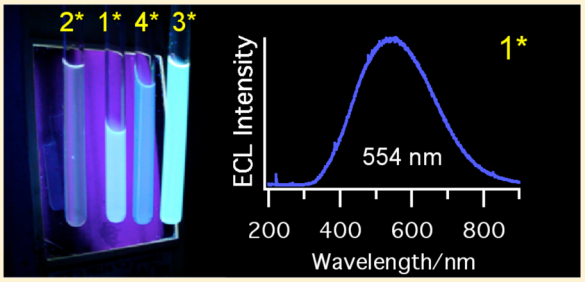

INTRODUCTION

Recently, there has been increasing interest in materials for electrochemiluminescent sensors and organic light-emitting diodes, OLEDs, for applications in television and lighting technology.[1] Organic luminescence is also a promising technology for the fabrication of flat panel displays.[2] The design of new luminophores has been driven by the requirement for RGB full color displays and white light illumination applications.[3−7] The emission color tuning in Alq_3, tris(8-hydroxyquinolinato)aluminum, analogues has been investigated with extended conjugated chromophores[8] and by modifying the N−O containing compounds by the addition of electron-withdrawing, EWG, or electron-donating groups, EDG.[3,8−10] Our group has studied the behavior of some triazole-modified deoxycytidine analogues in previous work.[11]

In this work, we synthesized and studied the spectroscopic properties and electrochemistry of four potential blue-emitting thienyltriazoles with N in the thienyltriazole ring and O in a methoxy or phenol group attached to the trizole acting as possible coordination atoms to form metal complexes. Our attention has been focused on designing modified thienyltriazoles to tune deep-blue fluorescence using "click chemistry".[12−15] The modulation of our thienyltriazoles is based on the reaction of azidothiophenes with terminal alkynes with a hydroxyl group to form a triazole ring, thus creating a fluorescent multiconjugated ring system with a hydroxyl group. Varying the conjugation in the thiophene ring system or adding a phenyl substituent between the thiophene-triazole backbone and the hydroxyl group might potentially modulate the ECL efficiencies before complexation with metals. Click chemistry with simple small molecules allows us to achieve the desired blue emission from the thiophene-triazoles (our first stage) while the hydroxyl group along with the triazole afford us potential N−O-containing metal complex emitters (our second stage). In this context, four thienyltriazoles, **1**−**4**, have been synthesized in this study as seen in Schemes 1 and 2. Note that our thienyltriazoles are blue luminescent.

Electrochemiluminescence or electrogenerated chemiluminescence, ECL, generates luminescence in solution,[16] while electroluminescent devices generate luminescence in the solid state. ECL involves light emission that is produced by an energetic electron-transfer reaction between electrochemically generated radicals in the vicinity of an electrode.[16] Two general methods for producing ECL are "annihilation" and "coreactant" reactions.[16] In annihilation systems, radical cations and anions are generated in solution and light emission results when they combine. Coreactant studies are useful when a system does not give stable radical cations or anions. Coreactant intermediates are either strong reducing agents in oxidative-reduction ECL or

Received: April 20, 2012
Published: June 5, 2012

   dx.doi.org/10.1021/jo300802h | *J. Org. Chem.* 2012, 77, 5646−5655

Scheme 1. General Procedure for the Synthesis of Thienyltriazoles 1 and 2 via Cu(I)-Catalyzed Huisgen 1,3-Dipolar Cycloaddition

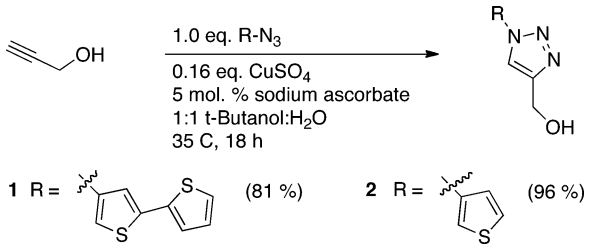

Scheme 2. General Procedure for the Synthesis of Thienyltriazoles 3 and 4 via Cu(I)-Catalyzed Huisgen 1,3-Dipolar Cycloaddition

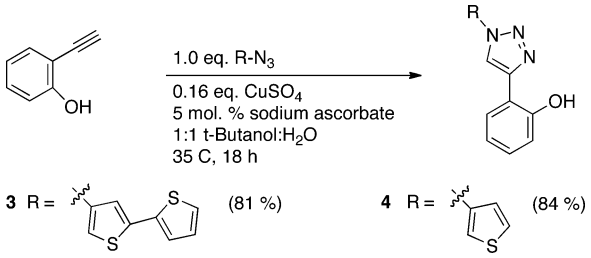

strong oxidizing agents in reductive-oxidation ECL.[16] Benzoyl peroxide (BPO) is a common coreactant and produces a strong oxidizing agent when reduced; this has been selected for the purpose of our studies.[16] Previously, we have studied the ECL of iridium(III) complexes containing aryltriazoles that emitted blue light.[17] We wanted to investigate if the prepared thienyltriazole ligands were electrochemiluminescent. Here, we report the electrochemical properties of **1**–**4**, their ECL spectra and efficiencies in annihilation and coreactant pathways, and correlations of structures and these properties. Furthermore, ECL[18−24] is of importance for possible applications in biosensors, OLED displays, optoelectronics, microelectronics, and bioanalytical chemistry.[1,3,18,20,25−30]

RESULTS AND DISCUSSION

Synthesis of Thienyltriazoles. Our focus has been on synthesis of thiophene-based luminescent molecules using the copper alkyne−azide cycloaddition, CuAAC, approach (click chemistry),[12−15] which chelates to Al and Zn for possible subsequent enhancement in fluorescence. The basic synthetic approach to our thienyltriazoles **1**–**4** has been outlined in Schemes 1 and 2. The triazole moiety links electron donor and acceptor units, leading to an inclusion of a luminescent emission via charge-transfer processes. The precursors were readily available and were easily converted to **1**–**4** using published procedures. In fact, compounds **1**–**4** were prepared using the "click" reaction between 3-azidothiophene, or 4-azido-2,2′-bithiophene, with 2-progargyl alcohol or 2-ethynylphenol. The "click" reactions had mild reaction conditions and required little product isolation and no chromatography. Stirring "click" reactions overnight at 35 °C resulted in high yields of **1**–**4** (81−96%). Recrystallization provided single crystals for **1**, **2**, and **4**, suitable for X-ray diffraction. The identities of **1**–**4** were confirmed by ^{1}H and ^{13}C{^{1}H} NMR spectra and HRMS. At this time, products **1**–**4** are new compounds.

Crystal Structures. An ORTEP representation of **1** has been shown in Figure 1a. The solid-state structure of **1** displays a high degree of planarity in the bithiophene ring system, with a torsion angle between the bithiophene rings, S(1)−C(1)−C(5)−C(6), of only 0.80°. There was twisting of the triazole ring system relative to the bithiophene ring system. A torsion angle of 41.42° around the ring junctions of C(8)−C(7)−N(1)−C(10) was observed between the triazole ring and its adjacent thiophene ring. In the solid state, molecules of **1** pack in a head-to-tail arrangement with their bithiophene ring systems approximately parallel and separated by a distance of 3.60 Å, between C(3) and C(6), Figure S1 (Supporting Information). When looking at three crystallographically adjacent molecules, there may be an H-bonding interaction between N(3) and the H-atom associated with O(1) a distance of 2.78 Å between the heavy atoms.

An ORTEP representation of **2** has been shown in Figure 1b. There was a high degree of planarity in the thiophene−triazole ring system of **2** with a small torsion angle of 4.10° between the

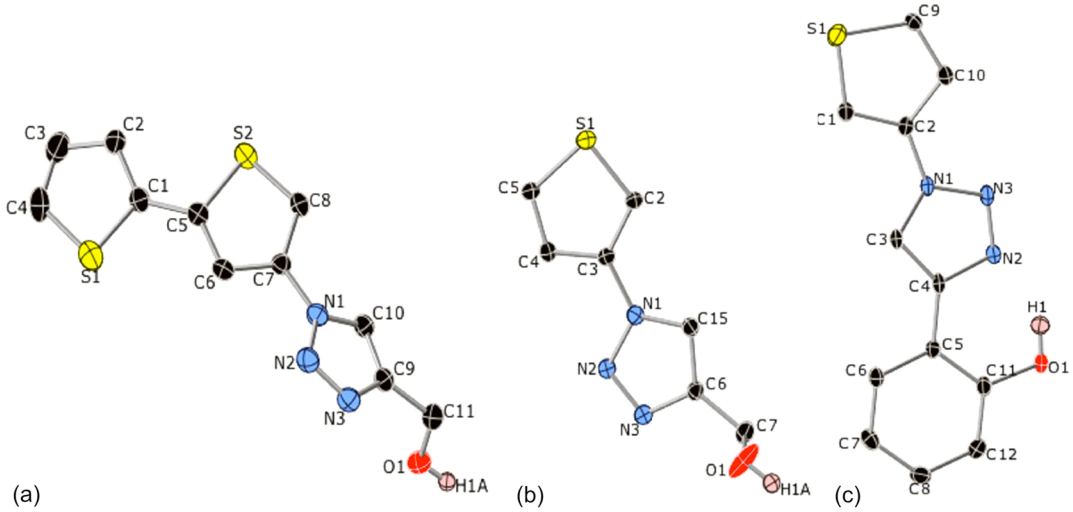

Figure 1. ORTEP representations of (a) **1**, (b) **2**, and (c) **4** (30% probability ellipsoids, H-atoms removed for clarity, expect −OH protons) with rings approximately parallel to the page.

dx.doi.org/10.1021/jo300802h | J. Org. Chem. 2012, 77, 5646−5655

two ring systems, C(3)−C(2)−N(1)−N(2). In the solid state, molecules of **2** pack in a head-to-tail arrangement with their ring systems approximately parallel and separated by a distance of 3.40 Å, between N(3) and C(15), Figure S2 (Supporting Information). There may be an H-bonding interaction between N(3) and the H-atom associated with O(1) from adjacent molecules with a distance of 2.81 Å between the heavy atoms.

An ORTEP representation of **4** has been depicted in Figure 1c. The molecules of **4** display a high degree of planarity throughout the three ring systems. There was probably an intramolecular hydrogen bond between one of the triazole N-atoms and the phenol OH group: the N(2)−O(1) distance was 2.63 Å, which was significantly less than the sum of the van der Waals radii of N and O (2.74 Å). The torsion angle between the thiophene and triazole rings C(1)−C(2)−N(1)−C(3) was 7.34° and the triazole and phenol rings N(2)−C(4)−C(5)−C(11) was 1.80°. In the solid state, molecules of **4** π-stack with all three ring systems approximately parallel and separated by a distance of 3.31 Å, between N(2) and C(10), Figure S3 (Supporting Information).

Electrochemistry and Its Correlation to Crystal and Electronic Structures. The cyclic voltammogram (CV) of **1** is shown in Figure 2 in acetonitrile solution containing 0.1 M tetra-*n*-butylammonium perchlorate as supporting electrolyte. When the potential was scanned from 0.000 to 2.740 V, **1** underwent oxidation at a peak potential of 1.828 V, becoming a radical cation. The oxidation process was irreversible in the CV since there was no return peak in the reverse potential scan from 2.740 to 0.000 V. Upon scanning in negative potential range, **1** was reduced to a radical anion showing a cathodic peak at −2.092 V. The radical anions were not stable as well since there was no anodic wave in the reverse potential scan. It should be noted that new peaks appeared in the middle of the potential window after one cycle of the potential scan. This indicated that some chemical reactions from the generated radicals occurred after the electrochemical reactions, which agreed well with their stabilities illustrated by the CV in Figure 2.

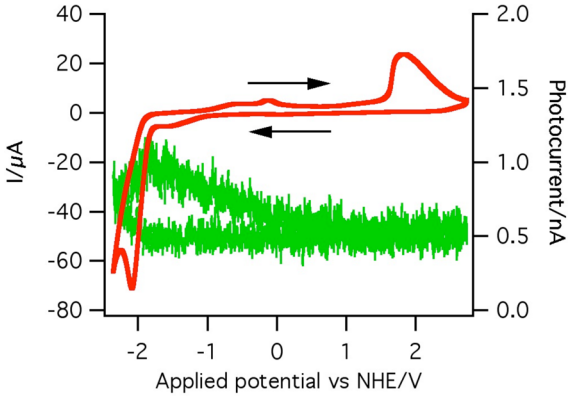

Figure 2. Cyclic voltammogram (red) and electrochemiluminescence−voltage curve (green) of **1** with a scan rate of 0.1 V s^{-1} and a potential range between 2.740 and −2.358 V.

In order to assess the redox property with less noise, differential pulse voltammetry (DPV) was used in the potential range of 2.810 and −2.289 V in the same supporting electrolyte, Figure 3. The formal potentials of **1** can be determined from eq 1,[31,32] where E_{max} is the peak potential in the DPV and ΔE is the pulse height (50 mV), we have estimated the potentials using the equation developed for a reversible system.

$$E^{0'} = E_{max} + \frac{\Delta E}{2} \quad (1)$$

Upon scanning the potential from −2.289 to 2.810 V, a peak potential was observed at 1.894 V for the oxidation reaction, top solid wave in Figure 3a, which was close to the peak potential obtained by CV. The formal potential for the oxidation was calculated as 1.919 V (Table 1) from eq 1. DPV provides better visibility than the CV in Figure 2 and could easily access the formal oxidation potential. As demonstrated from the crystal structure, Figure 1a, the bithiophene ring plane has a torsion angle as large as 41.42° relative the triazole ring. This led to a decrease in the conjugation length, a low delocalization of the charge upon losing an electron and therefore a low stability of the generated radical cation. Furthermore, we observed that the HOMO electron density of **1**, inset in Figure 3a, was distributed mostly on the bithiophene chromophore and minor on the triazole ring using density functional theory (DFT). The electron density extended less than expected from our molecule design on this conjugated ring system.

When the potential scanning direction was reversed, bottom solid wave in Figure 3a, a peak potential was observed at −1.905 V in the cathodic region, indicating the injection of an electron to the LUMO reduction reaction with a calculated formal reduction potential of −1.930 V (Table 1). The LUMO electron density again was delocalized on the bithiophene ring, inset in Figure 3a.

A small cathodic peak was observed in the cathodic DPV scan, top curve in Figure 3a, representing the instability of the radical cation. At the beginning of the DPV scan, radical cations were generated in the vicinity of the electrode. Upon scanning more negative, these anions, if they were still there, were rereduced to the neutral form. The lower peak current than that of the corresponding anodic peak in the anodic scan described well the irreversibility of the oxidation or the low stability of the radical cations. Similarly, a smaller anodic peak in the anodic DPV, top wave in Figure 3a, than that of the corresponding cathodic peak, bottom curve in Figure 3a, illustrated the irreversibility of the reduction or the low stability of the radical anions.

The electron promotion from HOMO to LUMO was delocalized mainly on the bithiophene, which might cause an inefficient luminescent emission. The electrochemical gap determined from the first oxidation and reduction potentials ($\Delta E = E_{ox}^{0'} - E_{red}^{0'}$) read 3.85 eV in Table 1, which agrees very well with electronic energy gap values of 4.03 eV in MeOH and 3.91 eV in DMF determined from UV−vis spectra, Table 2, and Figures S4−S5 (Supporting Information). It was noticed that the electrochemical gap could be obtained by differentiating the first oxidation and reduction peak potentials, which read 3.80 eV, very similar to that (3.85 eV) from the estimated formal redox potentials. The energy gap between the excited state and the ground state was evaluated from the photoluminescence spectrum, Figure S6 (Supporting Information), was 3.37 eV (Table 2), a value that was smaller than the electrochemical gap of 3.85 eV (Table 1). This implied a nonemissive relaxation from the electron promotion to the excited state.

Table 1 summarizes the electrochemical data of the other three thienyltriazoles, where their formal oxidation and reduction potentials are listed. The DPV of **2**−**4**, Figure 3b−

dx.doi.org/10.1021/jo300802h | J. Org. Chem. 2012, 77, 5646−5655

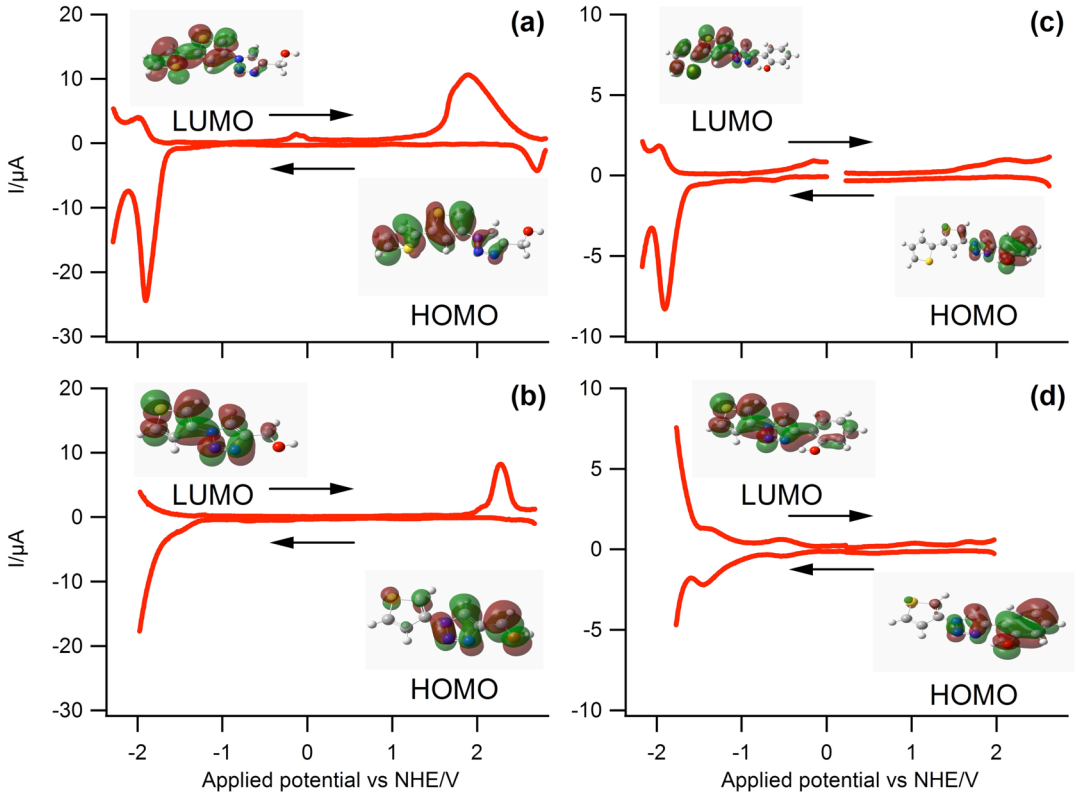

Figure 3. Differential pulse voltammogram and representations of the calculated HOMO and LUMO of (a) BiTTM (**1**) from 2.810 to −2.289 V, (b) TTM (**2**) from 2.683 to −1.976 V, (c) BiTTP (**3**) from 2.626 to −2.174 V, and (d) TTP (**4**) from 1.975 to −1.772 V in ACN containing 0.1 M TBAP as supporting electrolyte with a scan rate of 0.1 V s^{-1}. Gaussian-09 (B3LYP/6-31+G*) was used for calculations of **1**−**4** in hartrees/particle at T = 289.15 K, P = 1 atm.

Table 1. Redox Peak Potentials, Estimated Formal Potentials, and Electrochemical Gap along with HOMO−LUMO Energy Gaps Obtained by DFT Calculations

	$E_{p,a}$ oxidation[a] (V)	$E_{p,c}$ reduction[a] (V)	$E_{ox}^{0\prime a}$ (V)	$E_{red}^{0\prime a}$ (V)	ΔE^b (eV)	theor energy gap[c] (eV)
1	1.894	−1.905	1.919	−1.930	3.85	4.22
2	2.271	−1.524	2.296	−1.549	3.84	5.27
3	2.126	−1.906	2.151	−1.931	4.08	3.92
4	1.687	−1.460	1.712	−1.485	3.19	4.22

[a]In V vs Ag/Ag^+ at 0.1 V s^{-1} scan rate. [b]Energies determined from DPV first oxidation and reduction peak potentials data ($\Delta E = E_{ox}^{0\prime} - E_{red}^{0\prime}$). [c]Energy gap values obtained from the DFT/B3LYP/6-31+G* calculations.

Table 2. Absorption and Photoluminescence Spectroscopic Data of 1−4

	absorption		photoluminescence[a]			Stokes shift
	Abs λ_{max} (nm)	Abs (eV)	Ex λ_{max} (nm)	Em λ_{max} (nm)	Em[d] (eV)	λ_{max}(PL) − λ_{max}(Abs) (nm)
1	307[b] /313[c]	4.03/3.91	344	367	3.37	54
2	252[b]	4.92	366	453	2.73	201
3	302[c]	4.10	337	357	3.47	55
4	291[b]	4.26	337	358	3.46	67

[a]PL in MeOH. [b]Abs in MeOH. [c]Abs in DMF. [d]Energies determined from PL data.

d, shows irreversible oxidation and reduction processes in all cases. However, even though the processes were irreversible, the radical cations and anions were still generated in solution as seen from an increase in photocurrent in Figure 2. The irreversible processes led to great instability of the radical cations and anions, from which only a few excited species were generated through electron transfer. Ultimately, weak ECL was observed as a result. When the potential was scanned from −1.976 to 2.683 V in the electrolyte solution containing **2**, the radical cation was generated at a potential more positive than its formal potential for the oxidation reaction, estimated as 2.296 V, top solid wave in Figure 3b. The crystal structure showed very good planarity, and the HOMO electron density of **2** was delocalized on the thienyltriazole according to the DFT calculation, Figure 3b. However, **2** still showed a higher oxidation potential than **1**. This is because **1** might have a planar structure in solution and therefore a high degree of conjugation. Scanning from 2.683 to −1.976 V, **2** underwent reduction with a formal reduction potential of about −1.549 V, generating a radical anion of **2**, bottom solid wave in Figure 3b. The electron density for the LUMO of **2** was well delocalized on the thiophene and triazole rings and partially on the hydroxyl group, Figure 3b, leading a facile electron injection and therefore a less negative formal potential, −1.549 V, than that of **1**, −1.930. The HOMO−LUMO gap of **2** from the DFT calculation is 5.27 eV, Table 1, and is much higher than the electrochemical gap, 3.84 eV, but is compatible with the electronic gap from the absorption spectrum, Table 2 and Figure S4 (Supporting Information). The installation of the second thiophene ring in **1**, relative to **2**, shows a trend of

dx.doi.org/10.1021/jo300802h | J. Org. Chem. 2012, 77, 5646−5655

Table 3. ECL Spectroscopic Data of 1−4

	annihilation		coreactant			shift[b]
	scanning QE[a] (%)	pulsing QE[a] (%)	scanning QE[a] (%)	pulsing QE[a] (%)	λ_{max} (nm)	λ_{max}(ECL) − λ_{max}(Em) (nm)
1	0.11	0.00	0.50	0.40	544	185
2	0.17	0.00	0.16	0.01	554	91
3	0.50	0.00	0.35	0.08	546	189
4	1.11	0.01	0.40	0.02	422/576	84

[a]ECL quantum efficiencies (QE) measured in ACN relative to DPA (Φ = 6.1% in ACN).[36] [b]The shift represents the difference between the ECL and PL emission wavelengths in nm.

increasing conjugation resulting in a decrease in energy between the HOMO and LUMO, from 5.27 eV in **2** to 4.22 eV in **1** from Table 1. When looking at the electrochemical behavior of **2**, the electrochemical gap of 3.84 eV varied from its PL emission of 2.73 eV. This may be due to fast rotation between the thiophene and triazole rings, as seen in the disorder of the thiophene ring in the crystal of **2**.

For compound **3**, the radical cation formed when the potential was scanned from −2.174 to 2.626 V with its estimated formal oxidation potential of 2.151 V, top solid wave, Figure 3c. When the potential was scanned from 2.626 to −2.174 V, the radical anion was generated with its formal potential of about −1.931 V, bottom solid wave in Figure 3c. From the HOMO in Figure 3c, the electron density of **3** resided mostly on the bithienyltriazole ring system. In the LUMO, the electron density was delocalized on the phenol and triazole rings, with very little contribution from the bithiophene chromophore. From Table 1, we observed a decrease in the theoretical energy gap with the installation of the phenol ring to the bithienyltriazole compound. While the increase in conjugation in **3** decreased the energy gap from 4.22 eV in **1** to 3.92 eV in **3** based on DFT calculations, the electrochemical gap increased slightly from 3.85 to 4.08 eV. This discrepancy might be due to the planar geometry used in DFT calculations and incomplete planarity in electrolyte solution. For absorption, the energy was 4.10 eV, similar to the DFT energy of **3**, however there was no noticeable difference in energy between **1** and **3** for absorption. Compound **3** did not readily dissolve in MeOH, and was analyzed instead in DMF (see Figure S5, Supporting Information). Only one band was observed for both **1** and **3** due to the solvent cutoff of DMF at approximately 270 nm. The addition of the bithiophene and phenol aromatic systems to compound **3** increases the absorption intensities and selectively tunes the wavelengths relative to **1** and **2**. The electrochemical gap of **3**, 4.08 eV, was compatible with the electronic gap but larger than its PL emission energy of 3.47 eV. This again implies that nonemissive relaxation from the electron promotion to excited stated has occurred.

Lastly, compound **4** was scanned from −1.772 to 1.975 V, which generated the radical cation with its formal potential of 1.712 V, top solid wave in Figure 3d. From DFT, the HOMO electron density of **4** was delocalized on the entire compound, with the major contribution from the chromophore, very similar to that of **2**. The radical anion was formed when the potential was scanned from 1.975 to −1.772 V with its formal potential of −1.485 V, bottom solid wave, Figure 3d. The LUMO of **4** showed the electron density on the triazole and phenol rings. Comparing **2** with **4**, the theoretical energy gap of **4** was 4.22 eV, which was in good agreement with the absorption energy 4.26 eV, of **2**. From PL, the energy for **4** was 3.46 eV while the energy was 3.19 eV from the electrochemical gap of **4**. The decrease in energy between **2** and **4** was expected as we extended the conjugation in the compound. From DPV, we observed a decrease in the electrochemical gap of compound **2** of 3.84 eV to compound **4** of 3.19 eV. A decrease in energy was not observed between **1** and **3**, however this trend of decreasing energy with increased conjugation was seen between **1** and **2**.

ECL via Annihilation. In Figure 2, the CV of **1** is overlaid with the ECL photocurrent−voltage curve recorded simultaneously. Weak light emission from the thienyltriazoles during potential scanning was observed. The proposed mechanism for the observed ECL in **1** can be seen in eqs 2−5 and follows the annihilation pathway. When scanning from zero to positive potential, the radical cation of **1** was generated.

$$\mathrm{BiTTM} \rightarrow \mathrm{BiTTM}^{\bullet+} + \mathrm{e}^{-} \quad (2)$$

The potential was then scanned from the positive to the negative region. This generated the radical anion of **1** as seen in eq 3.

$$\mathrm{BiTTM} + \mathrm{e}^{-} \rightarrow \mathrm{BiTTM}^{\bullet-} \quad (3)$$

Through this annihilation pathway, the radical cation and anion generates an excited species of **1** and a ground-state species of **1**, eq 4. The excited thienyltriazole species will return to its ground-state and emit light, eq 5, as observed in the ECL photocurrent in Figure 2.

$$\mathrm{BiTTM}^{\bullet+} + \mathrm{BiTTM}^{\bullet-} \rightarrow \mathrm{BiTTM}^{*} + \mathrm{BiTTM} \quad (4)$$

$$\mathrm{BiTTM}^{*} \rightarrow \mathrm{BiTTM} + h\nu_1 \quad (5)$$

The ECL light was detected in the negative potential region. The stability of the radicals can be determined from where we observed light emission. The radical cations were more stable than the radical anions of this thienyltriazole compound because we only see ECL light after scanning from positive to negative potential. Compounds **2**−**4** demonstrated similar weak ECL emission.

Quantitatively, ECL efficiency can be calculated as the number of photons emitted per redox event relative to diphenylanthracene (DPA).[33−35] The ECL efficiencies were low, as seen in Table 3; however, the thienyltriazoles **1** and **3** displayed higher ECL efficiencies than **2** and **4** due to their extended π conjugation. The ECL efficiencies for compounds **1**−**4** were 0.11% for **1**, 0.17% for **2**, 0.50% for **3**, and 1.11% for **4**. CV of **1**−**4** shows irreversible processes indicating the poor radical stability.

Annihilation pulsing efficiencies were essentially zero, not efficient, because the radicals were not stable in solution as seen in the irreversible redox reactions, see Table 3. Since the compounds were not efficient through annihilation pulsing, the ECL spectrum for each compound was not obtained.

ECL via Coreactant. ECL was enhanced when BPO was added to the solutions of compounds **1**−**4** as observed in

dx.doi.org/10.1021/jo300802h | J. Org. Chem. 2012, 77, 5646−5655

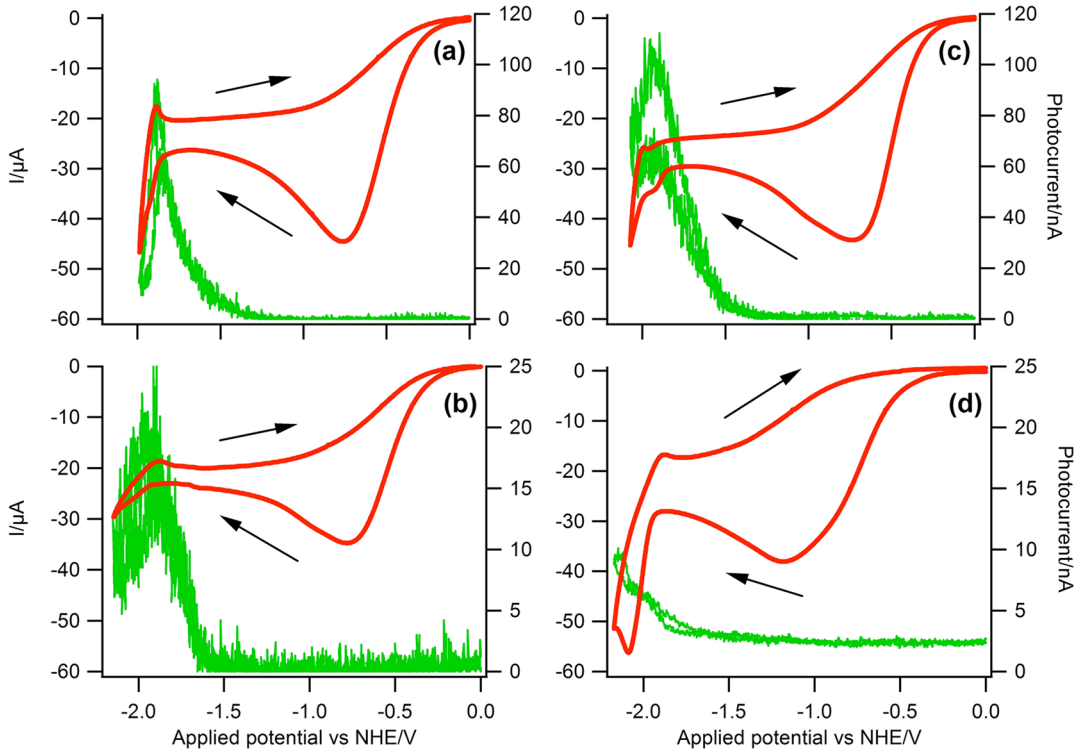

Figure 4. Cyclic voltammogram (red) and ECL–voltage curve (green) of (a) BiTTM (**1**) from 0.000 to −1.989 V, (b) TTM (**2**) from 0.000 to −2.145 V, (c) BiTTP (**3**) from and 0.000 to −2.074 V, and (d) TTP (**4**) from 0.000 to −2.021 V in ACN containing 5.0×10^{-3} M BPO and 0.1 M TBAP as supporting electrolyte with a scan rate of 0.1 V s^{-1}.

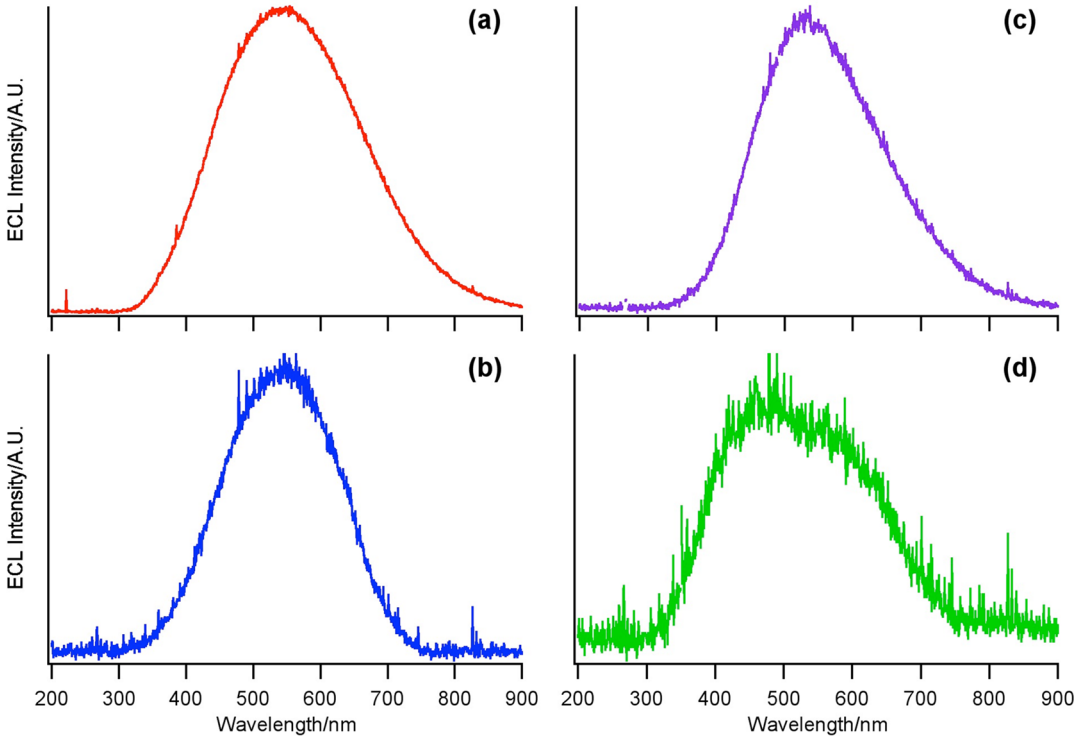

Figure 5. ECL spectra of **1**–**4** in ACN containing 5.0×10^{-3} M BPO and 0.1 M TBAP as supporting electrolyte, pulsing for t = 60 s between potential ranges from (a) 0.000 to −1.989 V for **1**, (b) 0.000 to −2.145 V for **2**, (c) 0.000 to −2.074 V for **3**, and (d) 0.000 to −2.021 V for **4**. ECL intensities were normalized by their respective peak heights.

Figure 4. Adding a coreactant to the solution was useful by generating ECL using a single potential step, one directional potential scanning at an electrode thus overcoming the limited potential window of the solvent, reducing the time dely for the meeting of radical anions and cations and therefore enhancing the ECL light emission by generating radicals in solution.[16,37]

dx.doi.org/10.1021/jo300802h | J. Org. Chem. 2012, 77, 5646–5655

The proposed mechanism for the observed ECL in **1**, Figure 4a, with BPO is stated in eqs 6−9 and follows the coreactant pathway. When scanning from 0.000 V to more negative potential, BPO was first reduced to its radical anion, $BPO^{\bullet -}$, at −0.760 V, as seen in eq 6.

$$BPO + e^- \rightarrow BPO^{\bullet -} \quad (6)$$

This radical rapidly decomposes to generate a strong oxidizing radical, $C_6H_5CO_2^{\bullet}$, eq 7.

$$BPO^{\bullet -} \rightarrow C_6H_5CO_2^- + C_6H_5CO_2^{\bullet} \quad (7)$$

In eq 8, the $C_6H_5CO_2^{\bullet}$ radical reacts with **1** and generates the radical cation of **1**, $BiTTM^{\bullet +}$.

$$C_6H_5CO_2^{\bullet} + BiTTM \rightarrow BiTTM^{\bullet +} + C_6H_5CO_2^- \quad (8)$$

Upon further reduction, the radical anion of **1** was observed at −1.883 V, eq 9.

$$BiTTM + e^- \rightarrow BiTTM^{\bullet -} \quad (9)$$

The radical cation and anion of **1** combine and form the excited species of **1**, BiTTM*, similar to eq 4 with the annihilation mechanism, and eventually relax back down to its ground state and light is emitted, eq 5.

A large increase in photocurrent in Figure 4a for **1**, approximately 90 nA, was observed using BPO. Comparing it to the photocurrent seen in annihilation, Figure 2, with approximately 1 nA, BPO significantly increased the amount of light detected. Compounds **2**−**4** in the same coreactant system showed increased intensities of photocurrent relative to that in the annihilation systems when extending the conjugation in the thienyltriazole ring system. ECL intensity generally increased with the addition of BPO to each system as seen in Table 3. Relative to the standard, DPA, a slight decrease in the efficiency appears. This was due to the fact that the efficiency of DPA was significantly higher with BPO relative to its efficiency without the coreactant. ECL was enhanced when using BPO and the efficiencies for compounds **1**−**4** were 0.50% for **1**, 0.16% for **2**, 0.35% for **3**, and 0.40% for **4**.

Pulsing experiments with coreactant resulted in slightly higher efficiencies than in the annihilation mechanism as seen in Table 3. When BPO was added to the solutions, there was a small increase in efficiencies for **1** at 0.40%, **2** at 0.01%, **3** at 0.08%, and **4** at 0.02% because pulsing generates the radicals faster therefore reducing the decay of the unstable radicals.

Being able to detect photocurrent even with these very low efficiencies allowed our group to acquire the ECL spectra for compounds **1**−**4** as seen in Figure 5.

ECL Spectra and Their Correlation to PL Spectra. The ECL spectra of compounds **1**−**4** containing BPO were obtained, Figure 5, and their peak wavelengths have been listed in Table 3. Pulsing between the potential ranges for each compound in the cathodic regions, thus reducing each compound, generated the excited species and the emission was acquired and recorded. The ECL spectra were red-shifted relative to the PL spectra as seen in Table 2. The ECL spectrum of **1** showed a maximum wavelength at 554 nm in ACN whereas its PL maximum was at 367 nm in MeOH. The difference of 185 nm could be due to the formation of excimers in solution during annihilation and coreactant studies.

It was possible that excimers form in solution because they were excited states of dimers that can be observed in ECL of organic compounds.[38,39] Excimers can form from dimerization of radical cations and anions or from stacking of the monomer in the ground state with one in the excited state due to the π conjugation of the compound.[33] When compound **1** was in solution with the excited species of **1**, BiTTM*, an excimer of **1**, $(BiTTM)_2$*, eq 10, could be generated.

$$BiTTM + BiTTM^* \rightarrow (BiTTM)_2^* \quad (10)$$

Another route would be the generation of the excimer of **1**, $(BiTTM)_2$*, when the radical cation and anion of **1** were in solution. Instead of generating an excited species of **1** and a ground-state species of **1**, as seen in eq 4, it could form the excimer of **1**, $(BiTTM)_2$*, eq 11.

$$BiTTM^{\cdot +} + BiTTM^{\cdot -} \rightarrow (BiTTM)_2^* \quad (11)$$

The excimer of **1**, $(BiTTM)_2$*, would relax down to its ground state and emit light as seen in eq 12.

$$(BiTTM)_2^* \rightarrow 2BiTTM + h\nu_2 \quad (12)$$

Excimer formation would be an alternate route the results in light emission. By changing the substituents on the compounds, adding an additional thiophene ring or by adding a phenol ring, the PL and ECL coreactant emissions were tuned based on the conjugated system. ECL peak wavelengths of **1** and **3** were the furthest red-shifted from their PL spectra. The ECL peak wavlength of **3** was observed at 546 nm with a red-shift of 189 nm relative to its PL peak wavelength. Compound **2** shows a red-shift of 91 nm and compound **4** demonstrates a red-shift of 84 nm. From Table 3, we can conclude that excimer formation was observed in each ECL system with BPO for all compounds studied when pulsing the electrode potential. The largest red-shift in wavelength was observed in **1** and **3**, the two compounds that had the bithiophene ring system. The addition of the phenol ring system to **4** changed the ECL excimer emission from 554 nm in **2** to 576 nm in **4**; thus, the extended conjugation in **4** increased the formation of excimers in solution for ECL measurements.

■ CONCLUSIONS

We synthesized four blue-emitting thienyltriazoles **1**−**4** that were characterized using ^1H and $^{13}C\{^1H\}$ NMR spectroscopy and high-resolution mass spectrometry. Crystal structures of **1**, **2**, and **4** were determined by X-ray diffraction. While **1** showed a torsion angle of 41.42° between the bithiophene and triazole rings, **2** and **4** possessed greater planarity. All four of the compounds underwent irreversible redox reactions to generate electrochemically unstable radical anions and cations. Based on DFT calculations, the majority of electron density resided on the chromophore for the LUMOs of **1**−**4**, and mostly in the triazole hydroxyl/phenol ring systems for the HOMOs, with the exception of the HOMO of **1**, where the electron density was delocalized on the bithienyltriazole ring system. Electrochemical gaps determined from the differences between first formal reduction and oxidation reactions correlated well to HOMO−LUMO energy gaps obtained from UV−visible spectroscopy and the DFT calculations as well as energies of excited states measured from photoluminescence spectroscopy. They demonstrated a trend dependent on the conjugation length and planarity. ECL efficiencies for annihilation of electrogenerated radicals were determined to be 0.11% for **1**, 0.17% for **2**, 0.50% for **3**, and 1.11% for **4**, relative to that of DPA. Upon addition of BPO as the coreactant, ECL intensities were enhanced approximately 90 times for **1**, 20 times for **2**, 100 times for **3**, and 10 times for **4**, bearing efficiencies of

dx.doi.org/10.1021/jo300802h | J. Org. Chem. 2012, 77, 5646−5655

0.50% for **1**, 0.16% for **2**, 0.35% for **3**, and 0.40% for **4**, relative to DPA in the coreactant system. The ECL spectra of **1**−**4** were acquired ranging from 544 nm for **1**, 554 nm for **2**, 546 nm for **3**, and 576 nm for **4**. The radicals electrogenerated in solution followed the dimerization and electron transfer pathways, leading to excimers. A red-shift was observed for all four compounds in the ECL spectra relative to the corresponding PL spectra. Monomer ECL emission was only observed for **4**. ECL is a valuable, quick, and cost-effective technique that requires a small quantity of compound while being highly sensitive and selective.

EXPERIMENTAL SECTION

General Methods. For synthesis and characterization, all reagents were purchased from commercial sources and used as supplied unless otherwise indicated. All experiments were conducted in air unless otherwise noted. Reactions that were carried out under an atmosphere of Ar were conducted using standard Schlenk techniques. Thin-layer chromatography was performed using 250 μm silica gel glass-backed plates and visualized by UV light. Flash column chromatography was performed using Silia*Flash* P60, 40−63 μm (D50) 60 Å, silica gel. All solvent mixtures were reported as volume ratios. Melting points were obtained using a Fisher-John melting point apparatus and reported uncorrected. The ^{1}H and ^{13}C{^{1}H} NMR data were recorded on a 400 MHz spectrometer at room temperature. High resolution mass spectrometry (HRMS) data were collected using electron spray (ESI) time-of-flight technique.

General Procedure for the Synthesis of Thienyltriazoles, 1−4, via Cu(I) Catalyzed Huisgen 1,3-Dipolar Cycloaddition. The following compounds were synthesized on the basis of previous literature: 3-azidothiophene,[30] 4-azido-2,2′-bithiophene,[30] and 2-ethynylphenol.[40] Compounds **1**−**4** were made by reacting either 2-propargyl alcohol (Scheme 1) or 2-ethynylphenol (Scheme 2) with one of the two corresponding thienylazides in the presence of a Cu(I) catalyst, from $CuSO_4$ and sodium ascorbate, in a 1:1 *tert*-butyl alcohol/H_2O solution. The products **1**−**4** were isolated and then purified for electrochemical and spectroscopic analyses and for X-ray crystallography of **1**, **2**, and **4**.

Synthesis of [1-(2,2′-Bithien-4-yl)-1*H*-1,2,3-triazol-4-yl]-methanol (1, BiTTM). To a solution of 4-azido-2,2′-bithiophene (0.80 g, 3.8 mmol), 2-propargyl alcohol (0.22 g, 3.8 mmol), and *tert*-butyl alcohol/H_2O (1:1, 6 mL) was added $CuSO_4$ (0.098 g, 0.62 mmol) at room temperature and the mixture stirred for 5 min. Sodium ascorbate (0.038 g, 0.19 mmol) was then added. The solution was initially yellow, and the reaction mixture was stirred overnight at 35 °C. After 16 h, the solution was yellow-brown. The product was extracted with ethyl acetate (3 × 10 mL) and washed with H_2O (3 × 10 mL). The combined organic phase, brown, was washed with ethyl acetate (10 mL) and brine (10 mL), dried ($MgSO_4$), and concentrated under vacuum to afford 0.82 g (81% yield) of **1**, light brown powder, mp 140−143 °C. HRMS: calcd for $C_{11}H_9N_3OS_2$ ([M]) 263.0187, found 263.0186.

Synthesis of [1-(3-Thienyl)-1*H*-1,2,3-triazol-4-yl]methanol (2, TTM). To a solution of 3-azidothiophene (0.064 g, 0.51 mmol), 2-propargyl alcohol (0.037 g, 0.66 mmol), and *tert*-butyl alcohol/H_2O (1:1, 2 mL) was added $CuSO_4$ (0.017 g, 0.11 mmol) at room temperature and the mixture stirred for 5 min. Sodium ascorbate (0.007 g, 0.03 mmol) was then added. The solution was initially yellow, and the reaction mixture was stirred overnight at 35 °C. After 16 h, the solution was yellow-brown. The product was extracted with ethyl acetate (3 × 10 mL) and washed with H_2O (3 × 10 mL). The combined organic phase, yellow, was washed with ethyl acetate (10 mL) and brine (10 mL), dried ($MgSO_4$), and concentrated under vacuum. The product was dissolved in ethyl acetate and methanol. Hexanes was added to the solution, which was left for recrystallization over a period of 5 days. This afforded 0.089 g (96% yield) of **2**, golden crystals, mp 127−130 °C. HRMS: calcd for $C_7H_7N_3OS$ ([M]) 181.0310, found 181.0308.

Synthesis of 2-[1-(2,2′-Bithien-4-yl)-1*H*-1,2,3-triazol-4-yl]-phenol (3, BiTTP). To a solution of 4-azido-2,2′-bithiophene (0.33 g, 1.6 mmol), 2-ethynylphenol (0.19 g, 1.6 mmol), and *tert*-butyl alcohol/H_2O (1:1, 12 mL) was added $CuSO_4$ (0.041 g, 0.25 mmol) at room temperature and the mixture stirred for 5 min. Sodium ascorbate (0.016 g, 0.079 mmol) was then added. The solution was initially yellow, and the reaction mixture was stirred overnight at 35 °C. After 72 h, the solution was yellow-brown. The product was extracted with ethyl acetate (3 × 10 mL) and washed with H_2O (3 × 10 mL). The combined organic phase, brown, was washed with ethyl acetate (10 mL) and brine (10 mL), dried ($MgSO_4$), and concentrated under vacuum. The product was dissolved in MeOH (10 mL) and then concentrated under vacuum to afford 0.42 g (81% yield) of **3**, light brown powder, mp 180−184 °C. HRMS: calcd for $C_{16}H_{11}N_3OS_2$ ([M]) 325.0344, found 325.0336.

Synthesis of 2-[1-(3-Thienyl)-1*H*-1,2,3-triazol-4-yl]phenol (4, TTP). To a solution of 3-azidothiophene (0.28 g, 2.28 mmol), 2-ethynylphenol (0.27 g, 2.28 mmol), and *tert*-butyl alcohol/H_2O (1:1, 10 mL) was added $CuSO_4$ (0.058 g, 0.36 mmol) at room temperature and the mixture stirred for 5 min. Sodium ascorbate (0.023 g, 0.11 mmol) was then added. The solution was initially yellow. After being stirred at 35 °C for 18 h, the solution turned brown-green with a precipitate. The product was extracted with ethyl acetate (3 × 10 mL) and washed with H_2O (3 × 10 mL). The combined organic phase, brown solution, was washed with ethyl acetate (10 mL) and brine (10 mL), dried ($MgSO_4$), and concentrated under vacuum to afford 0.46 g (84% yield) of **4**, light brown powder, mp 170−176 °C. HRMS: calcd for $C_{12}H_9N_3OS$ ([M]) 243.0466, found 243.0462.

Infrared Measurements. Infrared spectroscopy measurements were recorded using a Fourier transform infrared spectrometer; samples were run between KBr plates. The wavenumbers,values, were reported in cm^{-1}; peak intensities were given as follows: strong (s), medium (m), and weak (w).

UV−vis and Photoluminescence Measurements. UV−vis absorption (Abs) and photoluminecescnece (PL) spectra were recorded over the range of 200−800 nm using a fluorimeter with a xenon flash lamp and PMT detector interfaced to a computer workstation. Quartz cuvettes were used using a 1 cm path length cell at 25 °C. Spectroscopic grade methanol (MeOH) was used as received.

CV and ECL Measurements. For electrochemical studies, 9,10-diphenylanthracene (DPA, 97%), benzoyl peroxide (BPO, reagent grade, ≥98%), ferrocene (Fc, 98%), and supporting electrolyte, tetra-*n*-butylammonium perchlorate (TBAP, electrochemical grade) were used as received. All solutions were prepared using anhydrous acetonitrile (ACN, 99.8%) in a Sure Seal bottle that was immediately transferred into an N_2-filled drybox prior to use.

Electrochemical Preparation. Cyclic voltammetry (CV), differential pulse voltammetry (DPV), and electrogenerated chemiluminescence (ECL) experiments were conducted using a 2 mm diameter Pt disk inlaid in a glass sheath as the working electrode (WE), a coiled Pt wire as the counter electrode (CE), and a coiled Ag wire as the quasireference electrode (RE), respectively. Prior to each experiment, the WE was polished with a felt polishing pad using 1.0, 0.3, and 0.05 μm alumina suspensions for 5 min each to obtain a mirror surface that was then washed with copious amounts of deionized water. The WE was then electrochemically polished using a 0.1 M aqueous solution of H_2SO_4 by scanning 400 times between the potentials of 1.400 and −0.600 V at a scan rate of 0.5 V s^{-1} for a cleaner, more reproducible Pt surface.[28] Finally, the WE was rinsed with deionized water and then dried under a stream of Ar gas at room temperature. The CE and RE were rinsed with acetone, sonicated in acetone for 15 min, and then thoroughly rinsed with deionized water. The electrodes were dried at 100 °C for 5 min then left to cool to room temperature. The electrochemical cell was rinsed with acetone and deionized water, then immersed in a base bath of 5% KOH in isopropanol for 4 h, rinsed with deionized water, immersed in an acid bath of 1% HCl for 4 h, and then thoroughly rinsed with deionized water. The cell was dried at 100 °C overnight then cooled to room temperature. All solutions for electrochemical experiments were prepared in a glass electrochemical cell inside an N_2-filled drybox. The solutions of **1**−**4** ranged in

dx.doi.org/10.1021/jo300802h | J. Org. Chem. 2012, 77, 5646−5655

concentration from 2.0 to 2.7 × 10^{-3} M in ACN containing 0.1 M TBAP, the supporting electrolyte. For coreactant systems, 5.0 × 10^{-3} M BPO was added to each solution of **1**−**4**. These experiments were performed outside of the drybox. The electrodes were immersed in solution and connected by copper wire inserted through the cap. After completion of each experiment, the cell potential obtained was calibrated using Fc as the internal standard. The potentials were normalized to NHE using Fc/Fc^+. The redox potential of Fc/Fc^+ in ACN was taken as 0.400 V vs NHE.[41,42]

Electrochemical Instrumentation. CV is a technique that is used to measure the current during the process of linearly changing the potential between two limits on the working electrode at a given scan rate.[28] For all CV experiments, the potential windows range from 2.810 to −2.290 V for annihilation systems and from 0.000 and −2.150 V for coreactant systems. The experimental parameters for CVs were as followed: 0.000 V initial potential, positive or negative initial scan polarity, 0.1 V s^{-1} scan rate, 4 sweep segments, 0.001 V sample interval, 2 s quiet time, 1−5 × 10^{-5} AV^{-1} sensitivity. In DPV experiments, the differential current is taken as the current at the end of the pulse minus the current seen just prior to the pulse as the applied potential advances from one pulse to the next pulse.[31] For the purpose of our experiments, four DPVs were taken for each compound, two for anodic scans (0.000 to 2.810 V and 2.810 to 0.000 V) and two for cathodic scans (−2.290 to 0.000 V and 0.000 to −2.290 V), respectively. The experimental parameters for DPVs were as followed: 0.004 V increments, 0.05 V amplitude, 0.5 s pulse width, 0.0167 s sampling width, 0.2 s pulse period, 2 s quiet time, 1−5 × 10^{-5} AV^{-1} sensitivity.

ECL Instrumentation. The electrochemical cell had a flat Pyrex window at the bottom for detection generated from the WE and was sealed with a Teflon cap with a rubber O-ring for CV, DPV, and ECL measurements. The CV and ECL data were obtained using a electrochemical analyzer coupled with a photomultiplier tube (PMT) held at −750 V with a high voltage power supply. In the vicinity of the WE, ECL was generated and collected by the PMT under the flat Pyrex window at the bottom of the cell. The photocurrent from the PMT, which represents the ECL intensity, transformed this signal using a picoammeter/voltage source. The potential and current signals from the electrochemical workstation were sent through a data acquisition system (DAQ board) to the computer. The data acquisition system was controlled from a homemade LabVIEW program. The electrochemical cell was positioned inside the PMT to detect light emission for ECL pulsing experiments. The PMT was connected to the picoammeter/voltage source for signal conversion. A potentiostat was connected to an Universal Programmer. The data acquisition system was controlled from another homemade LabVIEW program. Current, potential and ECL signals were recorded simultaneously with the computer acquisition system. Pulsing the WE between the first oxidation and reduction peak potentials improved the ECL signals with a pulse width of 0.1 s or 10 Hz. The photosensitivity was set between 2 and 20 nA for annihilation systems and 200 nA for coreactant systems. The ECL spectra were obtained using a spectrometer containing a charge-coupled device (CCD) camera that was cooled to −55 °C prior to use and connected to the computer. Similar to the pulsing experiments, the samples were pulsed between the first oxidation and reduction peak potentials, between 0.000 and −2.150 V, at 10 Hz. The exposure time of the spectra was set to 60 s for coreactant systems. A program recorded the intensities. Vertical lines/spikes seen in the spectra were cosmic rays from the CCD spectrometer.

ECL Calculations. ECL quantum efficiencies (QE) were calculated relative to DPA (reported absolute ECL efficiencies of DPA = 6.1% in ACN)[36] by integrating both the ECL intensity and current value for each compound relative to the DPA standard, eq 13[33−35]

$$\Phi_x = 100\left(\frac{\int_a^b \mathrm{ECL}dt}{\int_a^b \mathrm{current}dt}\right)_x \Big/ \left(\frac{\int_a^b \mathrm{ECL}dt}{\int_a^b \mathrm{current}dt}\right)_{st} \quad (13)$$

where x = compound (**1**−**4**) and st = DPA.

Theoretical Calculations. The ground-state structures of **1**−**4** were optimized from the crystal structures, **1**−**3**, by using density functional theory[43] (DFT) with B3LYP/6-31+G* in hartrees/particle at T = 289.15 K, P = 1 Atm. Frequency calculations were also executed at the same level of theory as the optimizations, and the vibrational data confirmed that the structures were indeed true minima on the potential energy surface because there were no imaginary frequencies listed in the vibrational analysis. The crystal structure and optimized Cartesian coordinates of **1**−**4** have been given in the Supporting Information, Figures S8−S16.

■ ASSOCIATED CONTENT

Ⓢ Supporting Information

Crystallographic data, ^1H and $^{13}C\{^1H\}$ NMR spectra, mass spectrometry spectra, photophysical spectra, and Cartesian coordinates. This material is available free of charge via the Internet at http://pubs.acs.org.

■ AUTHOR INFORMATION

Corresponding Author

*Tel: 519-661-2111 x86161. Fax: 519-661-3022. E-mail: zfding@uwo.ca.

Notes

The authors declare no competing financial interest.

■ ACKNOWLEDGMENTS

We thank the Natural Sciences and Engineering Research Council (NSERC, Canada), Ontario Center of Excellence, and Canada Foundation for Innovation for generous financial support, Dr. R. H. E. Hudson, Dr. P. J. Ragogna, and Dr. D. W. Shoesmith for use of their instruments (The University of Western Ontario), Dr. Viktor N. Staroverov and Allison L. Brazeau for their assistance in using the Gaussian-09 program, X-ray Structures Western (Aneta Borecki), Mass Spectrometry (Doug Hairsine), SHARCNET, NMR Facility (Mathew Willans), and Electronics Shop (John Vanstone and Jon Aukema) for their quality technical service, and The University of Western Ontario and the Department of Chemistry for support of graduate research.

■ REFERENCES

(1) Tang, C. W.; Van Slyke, S. A. *Appl. Phys. Lett.* **1987**, *51*, 913.
(2) Shao, Y.; Qui, Y.; Hu, W.; Hong, X. *Adv. Mater. Opt. Electron.* **2000**, *10*, 285.
(3) Liao, S.-H.; Shiu, J.-R.; Liu, S.-W.; Yeh, S.-J.; Chen, Y.-H.; Chen, C.-T.; Chow, T.-J.; Wu, C.-I. *J. Am. Chem. Soc.* **2009**, *131*, 763.
(4) Kim, M. K.; Kwon, J.; Kwon, T. H.; Hong, J. I. *New J. Chem.* **2010**, *34*, 1317.
(5) Ichikawa, M.; Mochizuki, S.; Jeon, H. G.; Hayashi, S.; Yokoyama, N.; Taniguchi, Y. *J. Mater. Chem.* **2011**, *21*, 11791.
(6) Orselli, E.; Kottas, G. S.; Konradsson, A. E.; Coppo, P.; Frohlich, R.; Frtshlich, R.; De Cola, L.; van Dijken, A.; Buchel, M.; Borner, H. *Inorg. Chem.* **2007**, *46*, 11082.
(7) Malinauskas, T.; Daskeviciene, M.; Kazlauskas, K.; Su, H. C.; Grazulevicius, J. V.; Jursenas, S.; Wu, C. C.; Getautis, V. *Tetrahedron* **2011**, *67*, 1852.
(8) Pohl, R.; Anzenhacher, J., P. *Org. Lett.* **2003**, *5*, 2769.
(9) Wang, S. *Coord. Chem. Rev.* **2001**, *215*, 79.
(10) Chen, C. H.; Shi, J. *Coord. Chem. Rev.* **1998**, *171*, 161.
(11) Swanick, K. N.; Dodd, D. W.; Price, J. T.; Brazeau, A. L.; Jones, N. D.; Hudson, R. H. E.; Ding, Z. *Phys. Chem. Chem. Phys.* **2011**, *13*, 17405.
(12) Sharpless, K. B.; Kolb, H. C.; Finn, M. G. *Angew. Chem., Int. Ed.* **2001**, *40*, 2004.
(13) Kolb, H. C.; Sharpless, K. B. *Drug Discov. Today* **2003**, *8*, 1128.

(14) Wu, P.; Folkin, V. V. *Aldrichimica Acta* **2007**, *40*, 7.
(15) Wu, P.; Feldman, A. K.; Nugent, A. K.; Hawker, C. J.; Scheel, A.; Voit, B.; Pyun, J.; Fréchet, J. M. J.; Sharpless, K. B.; Folkin, V. V. *Angew. Chem., Int. Ed.* **2004**, *43*, 3928.
(16) Bard, A. J. *Electrogenerated Chemiluminescence*; Marcel Dekker: New York, 2004.
(17) Swanick, K. N.; Ladouceur, S.; Zysman-Colman, E.; Ding, Z. *Chem. Commun.* **2012**, *48*, 3179.
(18) Rosenthal, J.; Nepomnyashchii, A. B.; Kozhukh, J.; Bard, A. J.; Lippard, S. J. *J. Phys. Chem. C* **2011**, *115*, 17175.
(19) Shen, M.; Rodriguez-Lopez, J.; Huang, J.; Liu, Q. A.; Zhu, X. H.; Bard, A. J. *J. Am. Chem. Soc.* **2010**, *132*, 13453.
(20) Bandini, M.; Bianchi, M.; Valenti, G.; Piccinelli, F.; Paolucci, F.; Monari, M.; Umani-Ronchi, A.; Marcaccio, M. *Inorg. Chem.* **2010**, *49*, 1439.
(21) Ho, T. I.; Elangovan, A.; Hsu, H. Y.; Yang, S. W. *J. Phys.Chem. B* **2005**, *109*, 8626.
(22) Lai, R.; Fabrizio, E.; Lu, L.; Jenekhe, S.; Bard, A. *J. Am. Chem. Soc.* **2001**, *123*, 9112.
(23) Chen, Z.; Wong, K. M.-C.; Kwok, E. C.-H.; Zhu, N.; Zu, Y.; Yam, V. W.-W. *Inorg. Chem.* **2011**, *50*, 2125.
(24) Debad, J.; Morris, J.; Magnus, P.; Bard, A. *J. Org. Chem.* **1997**, *62*, 530.
(25) Miao, W. *Chem. Rev.* **2008**, *108*, 2506.
(26) Pyati, R.; Richter, M. M. *Annu. Rep. Prog. Chem., Sect. C* **2007**, *103*, 12.
(27) Richter, M. M. *Chem. Rev.* **2004**, *104*, 3003.
(28) Bard, A. J.; Ding, Z.; Myung, N. In *Structure & Bonding*; Springer: Berlin/Heidelberg, 2005; Vol. *118*, p 1.
(29) Li, Y.; Qi, H.; Yang, J.; Zhang, C. *Michrochim Acta* **2009**, *164*, 69.
(30) Dodd, D. W.; Swanick, K. N.; Price, J. T.; Brazeau, A. L.; Ferguson, M. J.; Jones, N. D.; Hudson, R. H. E. *Org. Biomol. Chem.* **2010**, *8*, 663.
(31) Bard, A. J.; Faulkner, L. R. *Electrochemical Methods, Fundamentals and Applications*, 2nd ed.; John Wiley & Sons: New York, 2001.
(32) Girault, H. H. *Electrochimie Physique et Analytique*; Presses Polytechniques et Universitaires Romandes: Laussane, 2001.
(33) Booker, C.; Wang, X.; Haroun, S.; Zhou, J.; Jennings, M.; Pagenkopf, B. L.; Ding, Z. *Angew. Chem., Int. Ed.* **2008**, *47*, 7731.
(34) Wallace, W. L.; Bard, A. J. *J. Phys. Chem.* **1979**, *83*, 1350.
(35) Laser, D.; Bard, A. J. *J. Electrochem. Soc.* **1975**, *122*, 632.
(36) Maness, K. M.; Bartelt, J. E.; Wightman, R. M. *J. Phys. Chem. A* **1994**, *98*, 3993.
(37) Ding, Z.; Quinn, B. M.; Haram, S. K.; Pell, L. E.; Korgel, B. A.; Bard, A. J. *Science* **2002**, *296*, 1293.
(38) Lai, R. Y.; Fleming, J. J.; Merner, B. L.; Vermeij, R. J.; Bodwell, G. J.; Bard, A. J. *J. Phys. Chem. A* **2004**, *108*, 376.
(39) Choi, J.-P.; Wong, K.-T.; Chen, Y.-M.; Yu, J.-K.; Chou, P.-T.; Bard, A. J. *J. Phys. Chem. B* **2003**, *107*, 14407.
(40) Acardi, A.; Cacchi, S.; Del Rosario, M.; Fabrizi, G.; Marinelli, F. *J. Org. Chem.* **1996**, *61*, 9280.
(41) Gagné, R. R.; Koval, C. A.; Lisensy, G. C. *Inorg. Chem.* **1980**, *19*, 2854.
(42) Koepp, H. M.; Wendt, H.; Strehlow, H. Z. *Elektrochem.* **1960**, *64*, 483.
(43) Frisch, M. J.; Trucks, G. W.; Schlegel, H. B.; Scuseria, G. E.; Robb, M. A.; Cheeseman, J. R.; Scalmani, G.; Barone, V.; Mennucci, B.; Petersson, G. A.; Nakatsuji, H.; Caricato, M.; Li, X.; Hratchian, H. P.; Izmaylov, A. F.; Bloino, J.; Zheng, G.; Sonnenberg, J. L.; Hada, M.; Ehara, M.; Toyota, K.; Fukuda, R.; Hasegawa, J.; Ishida, M.; Nakajima, T.; Honda, Y.; Kitao, O.; Nakai, H.; Vreven, T.; Montgomery, J. A., Jr.; Peralta, J. E.; Ogliaro, F.; Bearpark, M.; Heyd, J. J.; Brothers, E.; Kudin, K. N.; Staroverov, V. N.; Keith, T.; Kobayashi, R.; Normand, J.; Raghavachari, K.; Rendell, A.; Burant, J. C.; Iyengar, S. S.; Tomasi, J.; Cossi, M.; Rega, N.; Millam, J. M.; Klene, M.; Knox, J. E.; Cross, J. B.; Bakken, V.; Adamo, C.; Jaramillo, J.; Gomperts, R.; Stratmann, R. E.; Yazyev, O.; Austin, A. J.; Cammi, R.; Pomelli, C.; Ochterski, J. W.; Martin, R. L.; Morokuma, K.; Zakrzewski, V. G.; Voth, G. A.; Salvador, P.; Dannenberg, J. J.; Dapprich, S.; Daniels, A. D.; Farkas, O.; Foresman, J. B.; Ortiz, J. V.; Cioslowski, J.; Fox, D. J. *Gaussian 09 (Revision B.01)*; Gaussian, Inc.: Wallingford, CT, 2010.